

Detection of Slope Failures due to the Iwate-Miyagi, Japan Earthquake using Satellite Images

F. Yamazaki & T. Ishide

Department of Urban Environment Systems, Chiba University, Japan.



ABSTRACT

ALOS/AVNIR-2 optical images were employed to extract slope failures which occurred in the 14 June 2008 Iwate-Miyagi Inland, Japan, earthquake. Since the earthquake occurred in the mountainous area, many landslides were caused. In this paper, landslide areas were extracted comparing the pre- and post-event ALOS/AVNIR-2 images by two methods. One method uses the difference of the normalized difference vegetation index (NDVI) obtained from the pre- and post-event images. Another method performs a supervised land-cover classification by maximum likelihood approach, and the difference of extracted bare-ground pixels between the two images was recognized as landslide. The digital elevation model (DEM) was also employed to reveal the relationship between the slope angle and the occurrence of landslide, and to remove the extraction errors on non-sloping ground. Comparing with the visual inspection result, the accuracy of these image processing methods was demonstrated.

Keywords: the 2008 Iwate-Miyagi Inland earthquake, slope failure, ALOS/AVNIR-2, NDVI, DEM

1. INTRODUCTION

Satellite remote sensing is a powerful tool to capture various damages caused by natural disasters. Especially when a disaster strikes a mountainous region, the affected areas are very difficult to access at an early stage from the ground. The Mid-Niigata, Japan, earthquake ($M_J=6.8$) on October 23, 2004 and the Sichuan, China, earthquake ($M_w=7.9$) on May 12, 2008 are the typical examples. Various satellites captured the affected areas soon after the disasters struck (Rathje et al., 2006; Matsuoka et al., 2007; Miura and Midorikawa, 2008; Liu and Yamazaki, 2008) and the images from the various sensors were used for rescue operations and restoration planning.

A magnitude 7.2 (M_J) earthquake hit an inland region near the border of Iwate and Miyagi prefectures in the northern Japan on June 14, 2008 (Midorikawa and Miura, 2008). Since the epicenter is located in a mountainous region, the most roads in the affected region were blocked by slope failures/landslides and many villages were isolated. Hence, airborne and satellite, remote sensing technologies were employed to obtain damage distribution in this event (Geographical Survey Institute, 2008). As one of versatile satellites, ALOS (The Advanced Land Observing Satellite) captured the affected areas both before and after the earthquake by its AVNIR-2 and PALSAR sensors. In this paper, landslide detection is carried out using the pre- and post-event AVNIR-2 images based on the normalized difference vegetation Index (NDVI) and a supervised land-cover classification method.

2. THE 2008 IWATE-MIYAGI EARTHQUAKE AND ALOS/AVNIR-2 IMAGES

A strong earthquake hit the northern Honshyu (main) Island of Japan on June 14, 2008 at 8:43 AM (JST). The magnitude of the earthquake was $M_J=7.2$ and $M_w=6.9$. The Japan Meteorological Agency (JMA) determined the epicenter as $39^\circ 1.7' N$ and $140^\circ 52.8' E$ with the focal depth =14 km. A large number of strong motion records were obtained by this event, including the world largest PGA record

(about 3.9 g in the vertical component) at KiK-net (<http://www.kik.bosai.go.jp/>) Ichinoseki-West (IWTH25) station. In spite of such strong shaking in the source region, the damage to buildings was rather small because the region was mountainous and the buildings and houses were few: the number of severely damaged buildings was 30, moderately damaged 146, and with minor damage 2,521 (<http://www.bousai.go.jp/kinkyu/iwate2/2008-iwate-cao-033.pdf>).

Although the damage to buildings was not so large, a large number of landslides, rock falls, slope failures and debris flows occurred in the source region. Death tools and missing were counted as 23, mostly involved in debris flows and rock falls. Numerous landslides and slope failures were caused by this event and many roads and rivers in the region were blocked by them. And hence, the access to the affected area was very difficult from the ground.

Soon after the occurrence of the event, aerial damage surveys were conducted by Geographical Survey Institute (GSI) and private aerial survey companies. Since the affected region was vast and difficult to reach, various satellite sensors also tried to capture images. ALOS captured the affected areas both before and after the earthquake by its AVNIR-2 and PALSAR sensors. Figure 1 shows a part of ALOS/AVNIR-2 images taken (a) before and (b) after the earthquake, and the digital elevation model (DEM) of the study area with 50m grid-cell. The pre-event image was taken on October 17, 2006 at 10:53 am (JST) from the path No. 79 with the pointing angle 34.3° while the post-event image was taken on July 2, 2008 at 10:25 am (JST) from the path No. 67 with the pointing angle -2.5°. The AVNIR-2 images have four multi-spectral bands (B, G, R, NIR) with spatial resolution of 10 m. The co-registration of the two images and the DEM was carried out before image analyses.

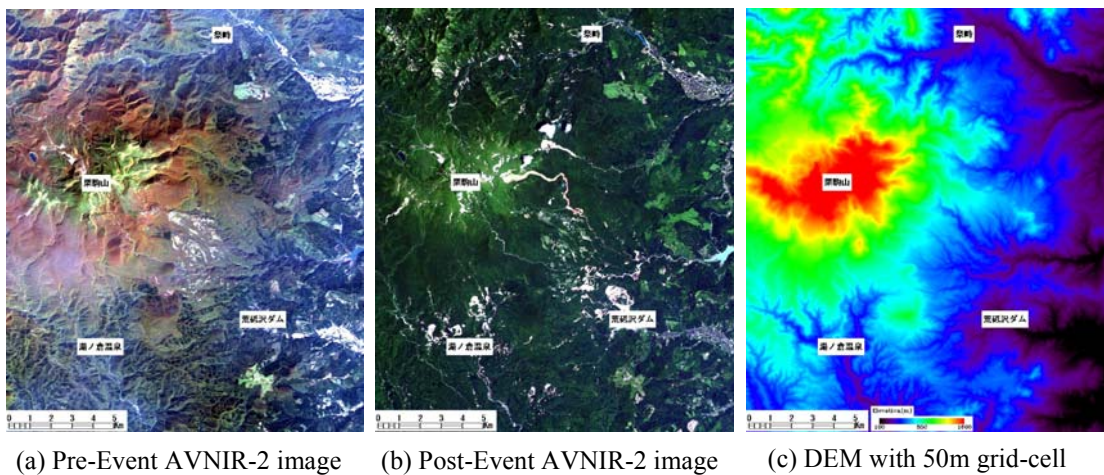


Figure 1. The pre-event and post-event ALOS/AVNIR-2 images and the DEM with 50 m grid-cell

2. EXTRACTION OF SLOPE FAILURES USING THE DIFFERENCE OF NDVI

To extract slope failures and landslides using the pre- and post-event AVNIR-2 images, the Normalized Difference Vegetation Index (NDVI) was calculated.

$$NDVI = \frac{NIR - R}{NIR + R} \quad (1)$$

where R is the digital number of the red band and NIR is that of the near-infrared band.

Figure 2 shows the NDVI values of the part of images near Aratozawa Dam, where the largest landslide occurred in the upstream of the dam. Comparing the NDVI values of the pre- and post-event images, the post-event NDVI value is seen to be much higher because the post-event image was taken in the early July (when the vegetation is most active in this region) while the pre-event image was taken in the mid October (when autumn foliage starts in highland).

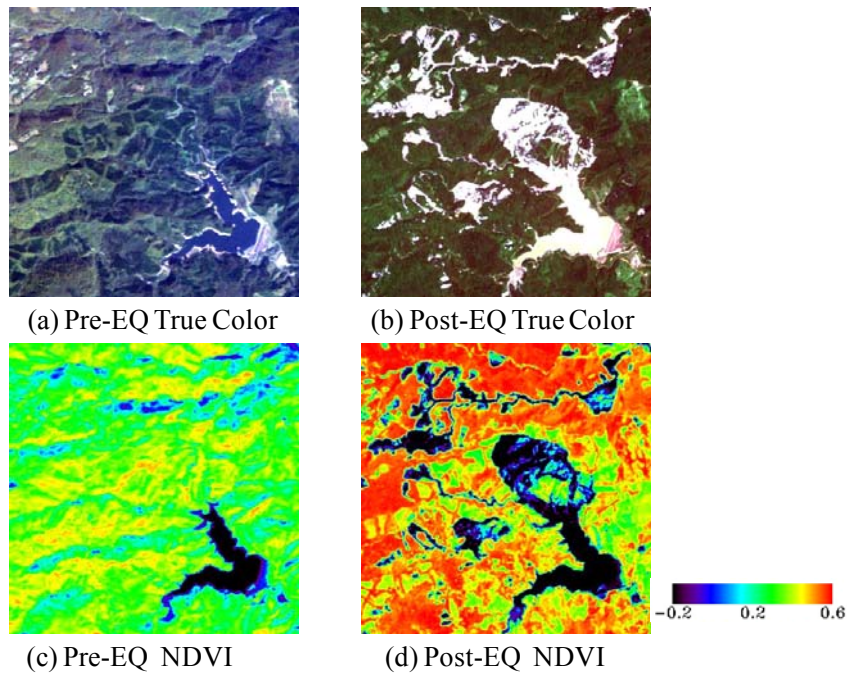


Figure 2. True color composite and NDVI images of Aratozawa Dam area

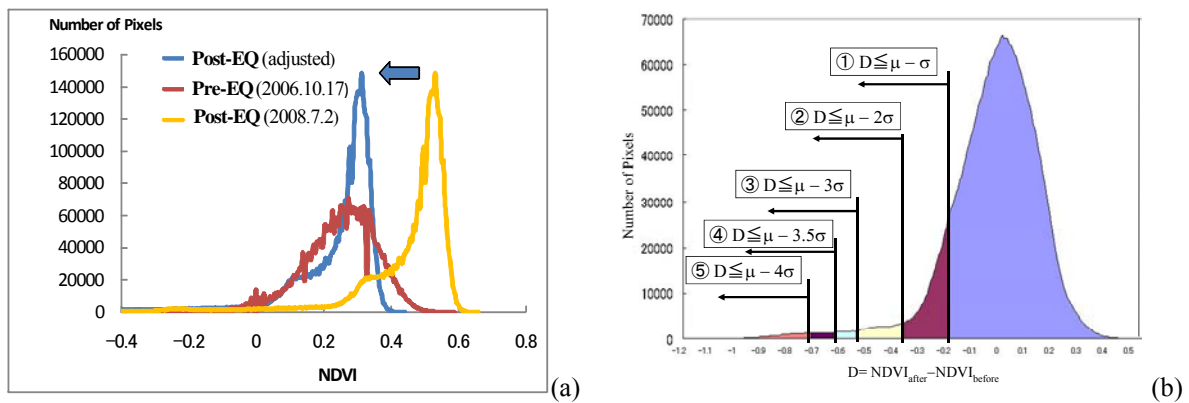


Figure 3. (a) The histograms of the pre- and post-event NDVIs and the adjusted post-event NDVI and (b) the histogram of the NDVI difference D after the adjustment

Figure 3 (a) plots the histograms of the NDVI value for the vegetated areas of the pre- and post-event images. Since the NDVI is higher in the post-event image, the post-event NDVI value was reduced (-0.217) so that the mean NDVI values of the two images in the vegetated area become equal. After this adjustment, the mean NDVI values became almost equal for the two images although the standard deviations are still different.

The difference (D) of the adjusted post-event and the pre-event NDVI values was calculated for each pixel and the histogram of the D value is shown in Figure 3 (b). The difference of the NDVI in time is considered to be caused by several factors, e.g. slope failure and landslide, the remaining seasonal change after the adjustment, the difference of sensor's view-angle. The distribution of the difference is seen to be non-symmetric with a long tail to the negative direction, which is consistent with the decrease of the NDVI due to slope failure/landslide. It is not easy to determine the threshold value to extract the change to bare-ground with other random variation. Thus following the previous studies (Yusuf et al. 2001; Miura and Midorikawa, 2008), the effect of the threshold value was examined by superposing the extracted pixels by different thresholds on the post-event image. The five threshold values shown in Figure 3 (b) were used to extract the earthquake-induced change and the results are plotted in Figure 4. Visual inspection of Figure 4 suggests that the area by $D \leq \mu - 2\sigma$ overestimates the

change while the area by $D \leq \mu - 3.5\sigma$ underestimates it. And hence, the area determined by $D \leq \mu - 3\sigma$ was considered as the earthquake-induced ground failures. Figure 5 (a) shows the extracted earthquake-induced change (62,422 pixels) for the entire study area by this method. The extracted area changes with the threshold value used, and thus the threshold value should be determined examining the balance of omission and commission errors (or the producer and user accuracy).

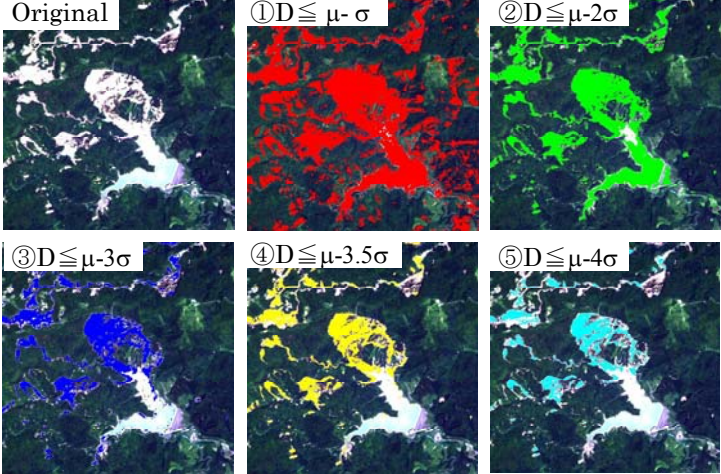


Figure 4. Extracted bare ground corresponding to the different threshold values of the difference of NDVIs

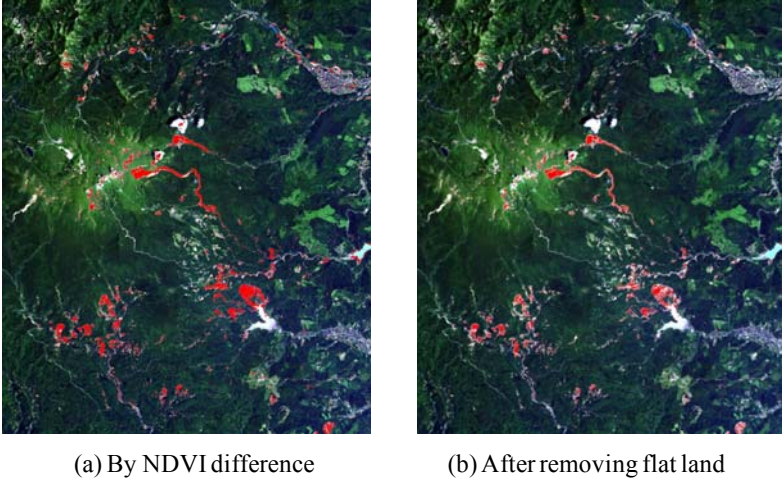


Figure 5. Extracted bare ground for the whole study area by the difference of NDVIs

3. EXTRACTION OF SLOPE FAILURES BASED ON LAND-COVER CLASSIFICATION

To extract the earthquake induced slope failures and landslides, another method based on land-cover classification was also carried out. A supervised classification by the maximum likelihood method was applied to the pre- and post-event images. To reduce errors in classification, the vegetated areas determined in the previous section were excluded in the classification. Then the pre-event image was classified into 4 classes: remaining vegetation, water body, village, and bare ground. In the similar manner, the post-event image was classified into five classes: remaining vegetation, water body, village, bare ground, and cloud. Note that some small clouds exist in the post-event image.

The results of supervised classification using the four multi-spectral bands are shown in Figure 6. As the bare ground class, 10,710 pixels were extracted for the pre-event image and 60,274 pixels for the post-event image. Out of these, 3,582 pixels were identified as bare ground both in the pre- and post-event times. Thus subtracting them from the post-event bare ground pixels, a total 56,692 pixels shown in Figure 7 (a) are estimated to belong to the earthquake induced slope failure/landslide.

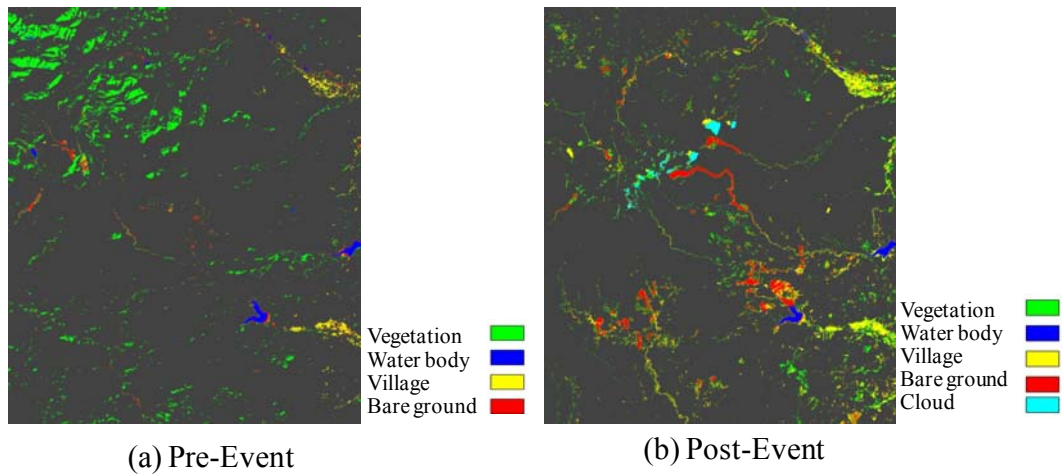


Figure 6. Land-cover classification for non-vegetated areas by the maximum likelihood method

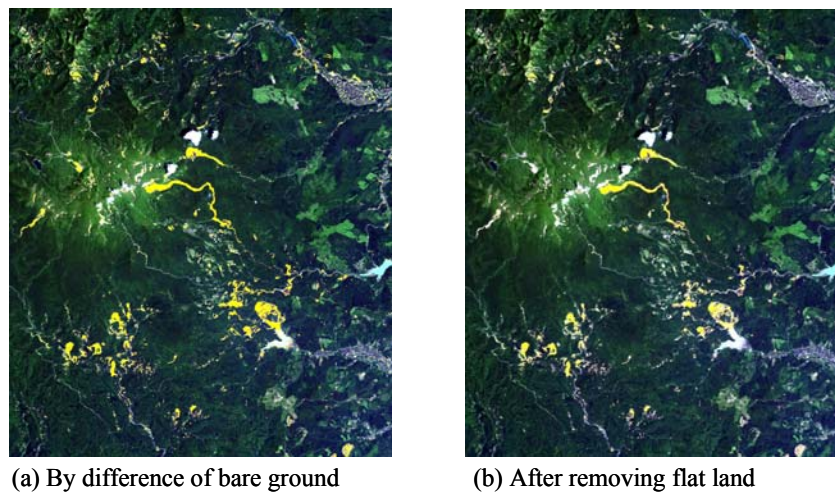


Figure 7. Extracted slope failures/landslides for the whole study area by land-cover classification

4. CHARACTERISTICS OF SLOPE FAILURES WITH RESPECT TO THE DEM

Comparing with the result of visual inspection, the extracted slope failures by the two methods are seen to be reasonable. However, some miss extracted pixels are observed in a flat land (village) and in a water body, as shown in Figure 8. These errors might be caused by the changes of crop in farms, the change of the water level and color, etc. The digital elevation model (DEM) with 50 m grid-cell was employed to remove flat lands from the extracted results.

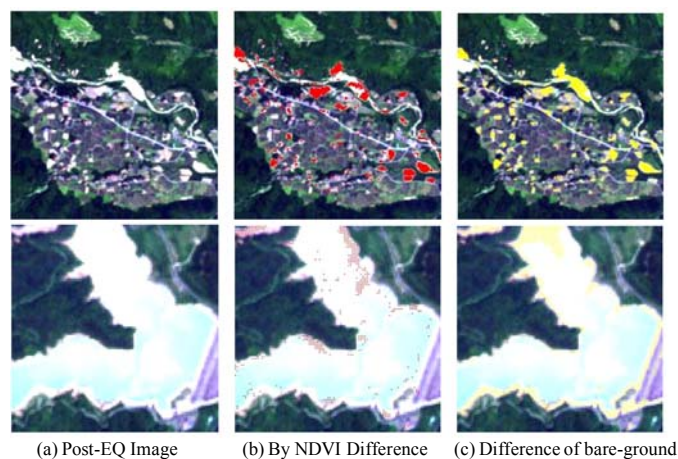


Figure 8. Examples of miss-extraction areas for a flat land (top) and a water body (bottom)

Using the DEM, the slope angle at the position of each pixel was calculated. Comparing the slope angle and the disaster situation map made from aerial photos (Geographical Survey Institute, 2008), the relationship between the slope angle and ground failure was investigated. Figure 9 shows the histograms of the slope angle for all the pixels, for the failed pixels, and the ratio of them. It is seen that the slope failure/landslide occurred mostly for the sloping ground between 30 to 60 degrees, and that the failure ratio increases as the slope angle increases. The similar trend have been observed in the Ikonos image of the 2004 Mid-Niigata, Japan, earthquake (Miura and Midorikawa, 2008) and the QuickBird image of the Sichuan, China, earthquake (Liu and Yamazaki, 2008). The detailed examination for the slope failures/landslides showed that they occurred for sloping grounds steeper than 10 degree. The previous studies (e.g. Miura and Midorikawa, 2008) also support this observation. Thus in this study, the flat lands with less than 10 degree were excluded to reduce commission errors.

Figures 5 (b) and 7(b) show the extracted results after removing the pixels with less than 10 degree. By this treatment, the total numbers of pixels extracted as slope failures were reduced to 52,313 for the NDVI method and 47,765 for the classification method. Figure 10 plots the result after removing the flat area for Figure 8. It is seen that the miss extractions in the farm have been eliminated correctly but that the errors in the water body still remain. This is due to the reason that the current DEM models the lake bed configuration as the ground surface, and hence the water body could not be removed.

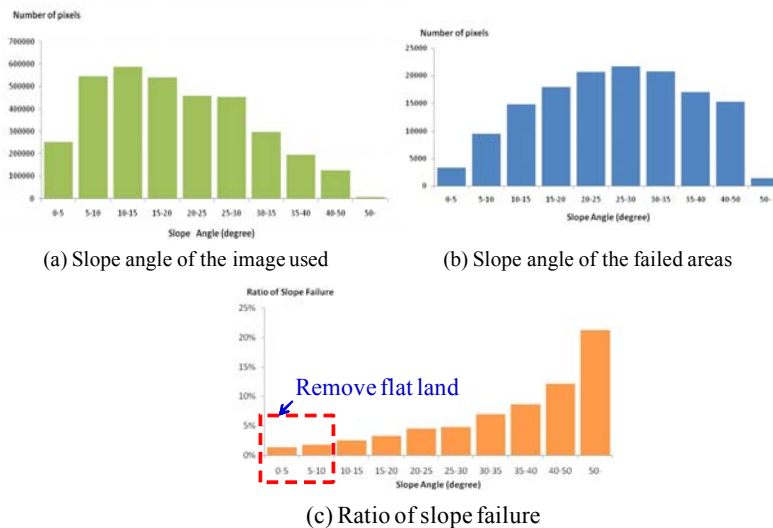


Figure 9. Histograms of the slope angle and the ratio of slope failure

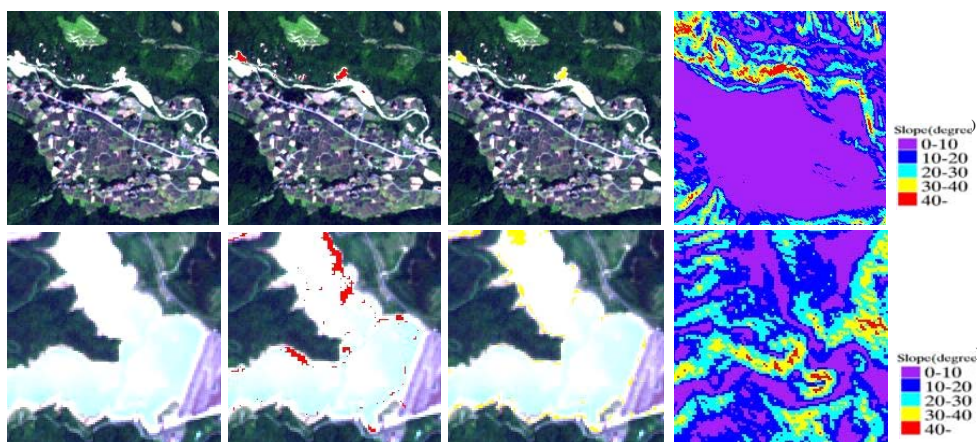


Figure 10. Removal of extracted areas less than 10 degree for flat land (up) and water body (down)

5. ACCURACY ASSESSMENT OF SLOPE FAILURE EXTRACTION

The results of the extraction after removing the low slope-angle pixels are shown in Figure 11, where the visual inspection result based on the aerial photographs (Geographical Survey Institute, 2008) is also plotted in blue lines. Since it is difficult to see details in Figure 11, the enlarged images are shown in Figure 12 for a heavily affected area: around Aratozawa Dam. It is seen that the bare grounds caused by slope failures and landslides well match with the automated extraction results.

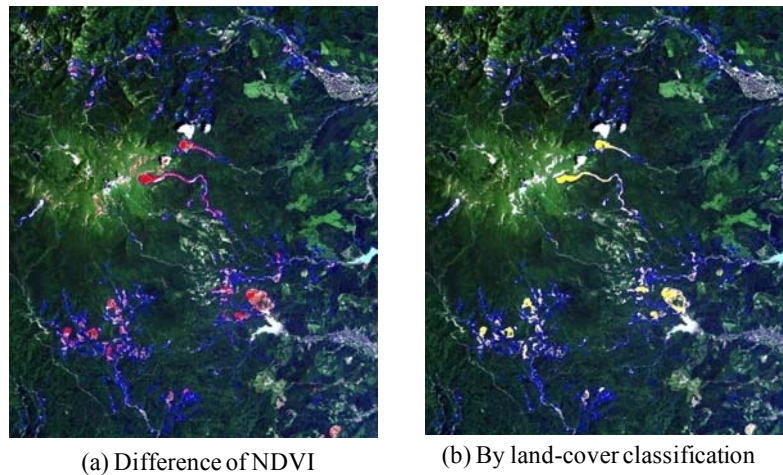


Figure 11. Comparison of the extracted slope failures after removing flat land and the visual inspection result (blue line)

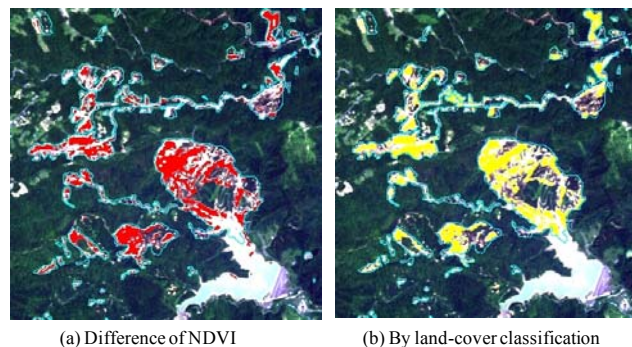


Figure 12. Comparison of the extracted slope failures after removing flat land and the visual inspection result (blue line) around Aratozawa Dam

A total of 707 slope failures and landslides were identified by the visual inspection. Table 1 shows the results of the image analyses and that of visual inspection in an object-basis, which means if the extracted pixels by the image analyses exist in a visually extracted slope failure/landslide, the extraction is considered to be a success for this location. The NDVI method could extract 470 locations correctly while 485 locations for the classification method. The accuracy of extraction is dependent on the scale of slope failure/landslide; if its area is larger than 500m^2 , almost 90% were extracted. On the contrary, if its area is smaller than 500m^2 , less than 50% were extracted by the both approaches. Considering the size of one image pixel of AVNIR-2 (100m^2), if the slope failure/landslide is larger than 5 pixels, it can be extracted with high accuracy.

The accuracy assessment was further conducted in a pixel basis. Table 2 shows the producer and user accuracies of extracted slope failures/landslides in terms of the number of pixels. The producer accuracy indicates the ratio of the extracted pixels out of the true (visual inspection) failure pixels. The user accuracy means the correctly extracted pixels out of all the extracted pixels. These accuracies are considered to be high by the two methods. The classification method gave better accuracy because this method uses all the 4 spectral bands and it requires the selection of proper training data.

Table 1. Object-based extraction results and the areas of slope failures

Area of slope failure	Number of slopes visually extracted	Extraction by NDVI	Extraction by classification
Less than 500m ²	373	178 (47.7%)	180 (48.3%)
More than 500m ²	334	292 (87.4%)	305 (91.3%)
Total	707	470 (66.5%)	485 (68.6%)

Table 2. Pixel-based extraction accuracy of slope failure areas

Accuracy	By NDVI	By classification
Producer Accuracy	68.2%	74.0%
User Accuracy	72.6%	86.2%

$\text{Producer Accuracy} = B/(B+C)$
 $\text{User Accuracy} = B/(A+B)$

6. CONCLUSIONS

Using the ALOS/AVNIR-2 images obtained before and after the 2008 Iwate-Miyagi, Japan earthquake, extraction of slope failures was carried out. Since the earthquake occurred in the mountainous area, many slope failures and landslides were caused. In this paper, slope failures and landslides were extracted comparing the pre- and post- event images of ALOS/AVNIR-2 by two methods. One method uses the difference of the normalized difference vegetation index (NDVI) obtained from the pre- and post-event images. Another method performs a supervised land-cover classification by a maximum likelihood approach, and the difference of extracted bare-ground areas between the two images is recognized as landslide. The digital elevation model was also employed to reveal the relationship between the slope angle and the occurrence of landslide and to remove extraction errors on the non-sloping ground. Comparing with the visual inspection result, the both image analyses methods gave good accuracy for the extraction of earthquake-induced ground failures.

REFERENCES

- Geographical Survey Institute (2008). <http://cais.gsi.go.jp/Research/topics/topic080625/index.html>
- JAXA (2008). http://www.eorc.jaxa.jp/ALOS/img_up/jdis_iwatemiyagi_eq_080702.htm
- Liu, W., Yamazaki, F. (2008). Damage Detection of the 2008 Sichuan, China Earthquake from ALOS Optical Images, *Proc. 28th Asian Conference on Remote Sensing*, Paper No. 119, CD-ROM, 6p.
- Matsuoka, M., Yamazaki, F. and Ohkura, H. (2007). Damage Mapping for the 2004 Niigata-ken Chuetsu Earthquake using Radarsat Images, *2007 Urban Remote Sensing Joint Event*, Paris, France, CD-ROM, 5p
- Midorikawa, S. and Miura, H. (2008). Damage and High-Resolution SAR Image in the 2008 Iwate-Miyagi-Nairiku, Japan Earthquake, *6th International Workshop on Remote Sensing for Disaster Applications*, Pavia, Italy.
- Miura, H. and Midorikawa, S. (2008). Detection of Slope Failure Areas Using IKONOS Images and Digital Elevation Model for the 2004 Niigata-ken Chuetsu, Japan Earthquake, *6th International Workshop on Remote Sensing for Disaster Applications*, Pavia, Italy.
- Rathje, E., Kayen, R. and Woo, K.-S. (2006). Remote Sensing Observations of Landslides and Ground Deformation from the 2004 Niigata Ken Chuetsu Earthquake, *Soils and Foundations*, **46: 6**, pp. 831-842.
- Yusuf, Y., Matsuoka, M. and Yamazaki, F. (2001). Damage Assessment after 2001 Gujarat Earthquake using Landsat-7 Satellite Images, *Journal of the Indian Society of Remote Sensing*, Photonirvachak, **29:1&2**, pp. 17-22.